Enhanced hot-electron localization and heating in high-contrast ultraintense laser irradiation of microcone targets

J. Rassuchine,[1] E. d'Humières,[1,7] S. D. Baton,[2] P. Guillou,[2] M. Koenig,[2] M. Chahid,[2] F. Perez,[2] J. Fuchs,[2] P. Audebert,[2] R. Kodama,[3,4] M. Nakatsutsumi,[4] N. Ozaki,[4] D. Batani,[5] A. Morace,[5] R. Redaelli,[5] L. Gremillet,[6] C. Rousseaux,[6] F. Dorchies,[7] C. Fourment,[7] J. J. Santos,[7] J. Adams,[8] G. Korgan,[8] S. Malekos,[8] S. B. Hansen,[9] R. Shepherd,[9] K. Flippo,[10] S. Gaillard,[1,10] Y. Sentoku,[1] and T. E. Cowan[1,11]

[1]*Department of Physics, University of Nevada, Reno, Nevada 89557, USA*

[2]*Laboratoire pour l'Utilisation des Laser Intenses, École Polytechnique, CNRS, CEA, UPMC, 91128 Palaiseau Cedex, France*

[3]*The Core Research for Evolutional Science and Technology (CREST), Japan Science and Technology Agency, Kawaguchi, Saitama 330-0012, Japan*

[4]*Graduate School of Engineering, Osaka University, 2-1 Yamada-oka, Suita, Osaka 565-0871, Japan*

[5]*Dipartimento di Fisica, Università di Milano-Bicocca, 20126 Milano, Italy*

[6]*Commissariat à l'Energie Atomique, 91680 Bruyères-le-Châtel, France*

[7]*CELIA, Université Bordeaux 1, 33405 Talance Cedex, France*

[8]*NanoLabz, 661 Sierra Rose Drive, Reno, Nevada 89511, USA*

[9]*Lawrence Livermore National Laboratory, P.O. Box 808, L-473, Livermore, California 94550, USA*

[10]*Los Alamos National Laboratory, Los Alamos, New Mexico 87545, USA*

[11]*Forschungszentrum Dresden-Rossendorf, P.O. Box 510119, 01300 Dresden, Germany*

(Received 3 July 2008; revised manuscript received 9 January 2009; published 31 March 2009)

We report experiments demonstrating enhanced coupling efficiencies of high-contrast laser irradiation to nanofabricated conical targets. Peak temperatures near 200 eV are observed with modest laser energy (10 J), revealing similar hot-electron localization and material heating to reduced mass targets (RMTs), despite having a significantly larger mass. Collisional particle-in-cell simulations attribute the enhancement to self-generated resistive (~10 MG) magnetic fields forming within the curvature of the cone wall, which confine energetic electrons to heat a reduced volume at the tip. This represents a different electron confinement mechanism (magnetic, as opposed to electrostatic sheath confinement in RMTs) controllable by target shape.

DOI: 10.1103/PhysRevE.79.036408 PACS number(s): 52.50.Jm, 52.38.Fz, 52.65.Rr, 52.75.−d

The production of hot, dense matter is important for studying extreme states of matter relevant to astrophysics [1] and inertial fusion [2,3]. In particular, direct laser heating has produced both strongly coupled plasmas [4] as well reached the highest temperatures [5], but only transiently (~ps) due to the rapid transport of the laser-generated fast electrons [6]. This leads to large spatial and temporal gradients of the energy deposition within the target, precluding a complete characterization of the plasma density and temperature. Several methods for producing more uniform isochorically heated matter are being explored including fast electron confinement by electrostatic sheath fields with reduced mass targets (RMTs) [7–10], as well as by external magnetic fields [11]. In addition, Sentoku *et al.* [12] predicted increased energy density with cone-shaped targets by the coupled effect of azimuthal magnetic and space-charge electric fields, which result in surface guiding of the superthermal (~MeV) electrons toward the tip.

Cone geometries are also extensively studied within the context of the fast ignitor (FI) approach to inertial fusion to improve laser conversion to hot electrons and ions closer to the compressed fuel [3,13]. Some experiments have reported enhanced optical collection [14–16] and K_α fluorescence [17] in large micromachined cones and heating of a wire attached to a cone [18]; however, the predicted wall-guiding [12] requires cones with sharper tips and small vertex angles. Moreover Baton *et al.* [19] found that under typical laser irradiation conditions, the amplified spontaneous emission (ASE) prior to the main pulse generates a large preformed plasma filling the cone, thereby inhibiting laser penetration to the cone wall.

In this paper, we present a different method of fast electron magnetic confinement incorporating microconical targets irradiated at high laser contrast. We observe enhanced conversion efficiencies and heating within a localized volume near the cone tip, which is deduced from K_α spectroscopy from highly charged Cu ions coupled with two-dimensional (2D) K_α imaging. Collisional particle-in-cell simulations attribute this enhancement to self-generated resistive magnetic fields (~10 MG) forming at the cone wall curvature, which effectively confine electrons below ~100 keV. Although the present work is not able to differentiate the predicted surface guiding, our observations are consistent with simulations of the magnetic field topology, electron transport, and heating dynamics.

The experiment was performed at the 100 TW laser at LULI with both 1ω ($\lambda=1.057$ μm) and frequency-doubled 2ω ($\lambda=0.53$ μm) light, where the respective estimated ASE contrast ratios were 10^{-7} and 10^{-12}. The laser pulse was focused with $f/3$ off-axis parabolas, resulting in a focal spot [full width at half maximum (FWHM)], energy and peak irradiance of 10 μm, 20 J and 1×10^{19} W/cm^2 at 1ω and 8 μm, 10 J, $4-8\times10^{18}$ W/cm^2 at 2ω. We irradiated 10 μm thick freestanding Cu cones with tip diameters (4–25 μm) and shapes ranging from sharp to an extended funnel. We will focus on the funnel geometry (5 μm inner

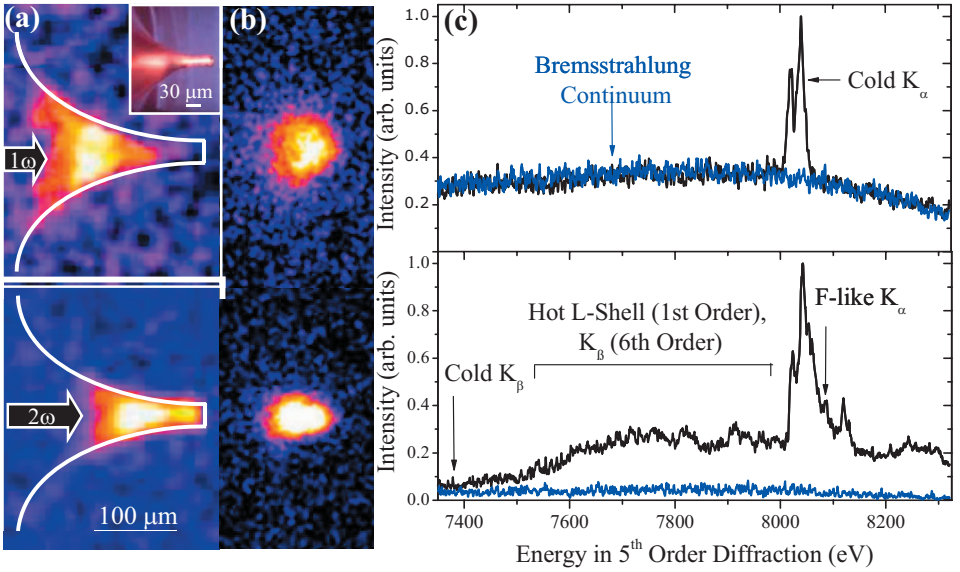

FIG. 1. (Color) (a) Transverse and (b) rear-side images and (c) spectral emission of the K_α band of a funnel cone (inset) at 1ω (top row) and 2ω (bottom row) indicate the effect of a preplasma on laser propagation, hot-electron localization, and heating within the cone tip.

tip diameter), which gave the most pronounced laser-cone coupling, extending ≈ 195 μm from a 325 μm base diameter above a 2×2 mm supporting foil. As a comparison, planar 50–300 μm diameter multilayered (V-Cu-Al) RMTs were studied, with the laser irradiation at normal incidence on the V layer.

The time-integrated Cu K_α emission was spatially resolved by Bragg crystal imagers [20] in both the transverse and rear-side (90° and 30° from laser-cone axis) direction to monitor hot-electron propagation toward the cone tip [21]. A high-resolution conical crystal spectrometer [22] viewing downward on the nonirradiated surface of the target at 45° from the laser-cone axis was used with a spectral range viewing Al K_α in first-order Bragg diffraction (7.45–8.45 Å) and the Cu K_α in fifth order for K_α spectroscopy [23]. Heating of the Cu target material shifts the ionization balance to higher Cu charge states, resulting in a blueshifted K_α spectra, which yields information on the ionization state of a dense plasma [8].

Figure 1 presents the laser interaction with a funnel cone both with (1ω) and without (2ω) the presence of a preplasma. Both K_α images indicate peak hot-electron generation occurs ~ 50 μm deeper into the cone at 2ω versus at 1ω, with a corresponding $\sim$3-fold higher K_α yield within a reduced radial extent (twofold smaller FWHM). This reflects improved conversion of the 2ω light, which interacts directly with the dense cone wall along its path toward the tip. In addition, it implies a confinement of the electrons at the cone curvature which may be explained by the finite laser spot size and the lower energy of the laser-generated electrons at the oblique laser-cone incidence, inducing a strong temperature gradient and exciting resistive magnetic fields.

Comparatively, the spatially integrated spectra [Fig. 1(c)] at 1ω versus at 2ω display a significant diffuse background not focused by the conical crystal (blue curves), which is presumably from energetic bremsstrahlung x rays associated with electron acceleration to multi-MeV energies within a large preplasma [24]. Utilizing the atomic kinetic code FLYCHK [25], we estimate from the K_α line shape, an average temperature of the solid density Cu target ($n_{\mathrm{ion}}=8.4\times 10^{21}$ cm^{-3}) of ~ 45 eV for the 1ω data. The 2ω data show a reduced background, but with a broader and more complex K_α spectrum.

Although a precise fit to the entire 2ω spectrum is not feasible due to the temporal evolution of the target heating and the expected spatial gradients, we do observe short-wavelength satellites through the $n=3$ shell to Ne-like Cu^{19+}, which from FLYCHK [25] indicates peak bulk Cu temperatures of order 200 eV at solid density. The broad manifold of several unresolved transitions underlying the K_α emission likely corresponds to L-shell (3–2) transitions from unfiltered first-order crystal diffraction with a possible weak K_β signal in sixth order. Subsequent experiments have distinguished first from higher order diffraction, indicating that the L-shell continuum originates from a dense surface plasma with temperatures exceeding several hundred electron volts. We also

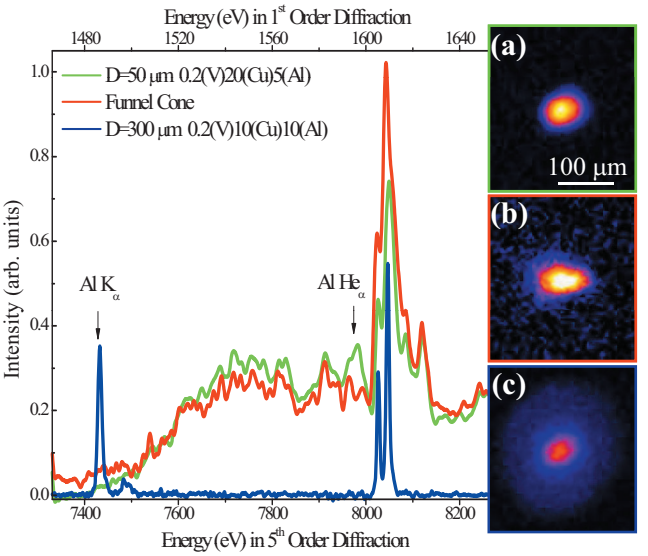

FIG. 2. (Color) Spectral (main plot) and rear-side (right column) K_α emissions of a (a) 50 μm diameter RMT, (b) funnel cone, and (c) 300 μm diameter RMT at 2ω compare heating and electron localization.

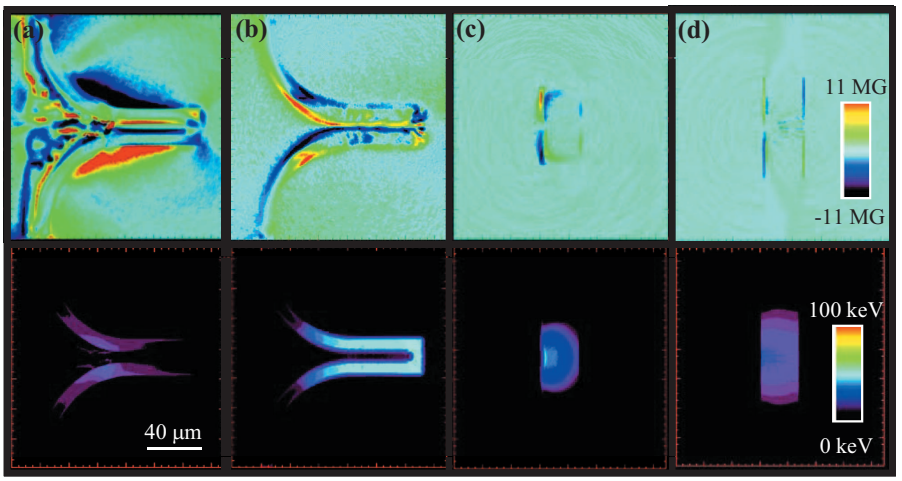

FIG. 3. (Color) Collisional PIC simulations of the magnetic field (upper panel) and the electron energy density (lower panel) for a funnel cone (a) with preplasma at 1 ps after the laser interaction and (b) without preplasma after 2 ps, and (c) a 50 μm and (d) 300 μm diameter RMT. At high contrast, the cone exhibits strong resistive fields (>10 MG) within the cone wall, which confine the ~100 keV electrons to the tip.

tested whether the enhanced heating at 2ω was due to the lower mean energy of the laser-generated electrons [6] by reducing the laser intensity (energy) at 1ω to match the predicted T_{hot} at 2ω [26]. We observed no increase, but rather a significant reduction in the K_α yield. We conclude that the enhanced heating at 2ω is from improved laser penetration and coupling at solid density.

In order to investigate the efficacy of the microcone for material heating, the spectral and rear-side K_α emissions from a funnel cone are compared to multilayer (V/Cu/Al) planar reduced mass targets (RMTs) at 2ω (Fig. 2), revealing a strong dependence on heating with target size and geometry. The 300 μm diameter RMT exhibits a typical "cold" spectrum with well-resolved Cu and Al K_α lines; whereas the 50 μm diameter RMT exhibits "hot" Cu K_α emission as well as a strong L-shell component, indicative of higher temperatures. Comparatively, the funnel cone spectrum exhibits similar heating as the 50 μm RMT. The increased heating with decreasing RMT volume is consistent with other works [8–10] reflecting the ambipolar sheath field confinement of the hot (~MeV) electrons.

The remarkable similarity of the spectra from the Cu funnel cone and the 50 μm RMT empirically implies similar peak temperatures. The ~40-fold larger Cu mass of the cone versus the 300 μm cold RMT implies there is a confinement mechanism for the hot electrons, which locally heats the cone tip within a volume akin to the 50 μm RMT. The rear-side K_α images (right panel in Fig. 2) show an indication of this localization. The 300 μm RMT target exhibits the bright central laser spot surrounded by a halo of electron diffusion. In comparison, the cone appears similar in intensity and spatial dimension to the 50 μm RMT, with little emission beyond the tip. A quantitative measure of conversion efficiencies is complicated by self-absorption from increased opacity of K_α emission above 100 eV, but normalizing to the Cu emitting volume and laser energy, the funnel cone exhibits 1.9–2.3 times higher coupling in terms of K_α yield.

To identify the mechanism responsible for the observed electron localization and heating, we used advanced collisional 2D collisional particle-in-cell (PIC) simulations to investigate the field structure and energy deposition resulting from the laser-generated superthermal (~MeV) and (~keV) hot-electron transport. Distinct from previous collisionless simulations investigating surface guiding [12], our code (PICLS) utilizes a binary collision module extended to correctly treat both relativistic collisions and collisions between weighted macroparticles [27]. Simulations do not model the three-dimensional (3D) filamentation of the hot-electron beam nor the 3D topology of the resistive magnetic fields [28,29].

The simulations assume a Gaussian (temporal and spatial) laser pulse (p polarization, $\lambda=1$ μm, 350 fs, 10 μm FWHM) injected from the left of a 150×150 μm simulation box. The peak of the pulse reaches the cone 500 fs after the beginning of the calculation. Neglecting ionization processes, we assume the Cu target is fully ionized with 4 Cu ions and 116 electrons within each cell on the mesh ($\Delta x=\Delta y=80$ nm). The initial electron temperature is zero, and the time step is 0.26 fs. In order to model the interaction of a pulse with a solid target and to ensure that the laser does not

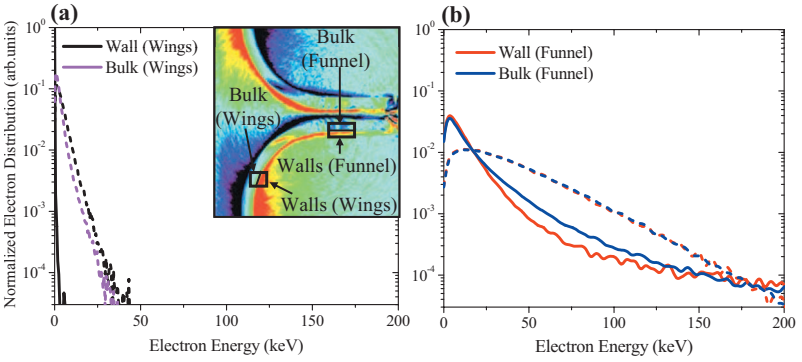

FIG. 4. (Color) The electron energy distribution at the maximum laser energy deposition (solid curve) and at 1.3 ps later (dashed curve) of a funnel cone at: (a) the wings of the wall (black curve) and bulk (magenta curve) and in the (b) neck wall (red curve) and bulk (blue curve). This reflects the lower energy part of the electron spectrum being confined to the tip by the resistive wall fields and the shift to higher energies in the bulk electron population by heating.

propagate inside the target, we chose a target density of $10n_c$, higher than the relativistic critical density, $a_0 n_c = 2n_c$, where a_0 is the normalized laser amplitude and n_c is critical density ($n_c = 1.1 \times 10^{21}/\lambda\ (\mu\text{m})^2\ \text{cm}^{-3}$). Our simulation also includes a Monte Carlo Coulomb scattering for the electron transport inside the target using the full ionization state Z. Although the ionization, which affects the collisionality (and resistivity), is not treated self-consistently, approximate values for the effective Z^* are based on the observed peak T_e deduced from spectroscopy: $Z^* = 29^+$ for the "hot" funnel cone and 50 μm RMT and $Z^* = 7^+$ for a larger 150 μm diameter "cold" RMT. Thus, our model overestimates the collision frequency in the calculation, but it also underestimates the resistive field strength by adopting an artificially low density. Nevertheless, the resistive magnetic fields we see in these simulations are in the reasonable range with previous simulations, which verified the resistive field in a laser heated target using a reduced density in a comparison of the full density simulation via PICLS [27].

Figure 3 compares a 10 μm thick Cu funnel cone irradiated with and without a preformed to 50 and 150 μm diameter (27 μm thick) RMTs. The upper panel gives the magnetic field distribution at 1 ps [Fig. 3(a)] and 2 ps [Figs. 3(b)–3(d)] after the arrival of the laser pulse. The lower panel plots the average electron energy density, which includes the small fraction of hot electron responsible for producing K_α emission and the average temperature of the heated bulk responsible for the Cu ionic state and *L*-shell emission. Without a preplasma, the funnel cone excites strong (~10 MG) magnetic fields along the surfaces and within the curvature of the cone wall. The localized resistive field results from the lower-energy electrons generated at near-normal interaction at the cone curvature, which, in combination with a finite laser spot [30], can result in a large temperature gradient. These fields effectively confine hot electrons (~100 keV), which are then distributed throughout the tip, locally heating a reduced volume. In contrast, when the cone is filled with a preplasma (estimated scale length of 120 μm, ranging from 0.3 to $3n_c$) the laser filaments and is absorbed before reaching the walls. The well-localized resistive field is replaced by an extended surface field, indicative of the larger range of ~MeV electrons. The planar RMT foils exhibit weaker surface and resistive fields, as the fast electron flow extends throughout the entire planar volume.

The resistive magnetic cone-wall fields appear to be the mechanism resulting in a predicted fourfold higher coupling of laser energy to hot electrons with the funnel versus planar targets. They persist for ≥ 6 times longer than the laser pulse, inhibiting the transport of ~100 keV electrons away from the tip. Comparatively, the strong magnetic and sheath surface fields pull escaping electrons back, forming surface currents, which complicate the spatial distribution of heating in the funnel. Figure 4 shows snapshots from the funnel cone simulation without preplasma of the electron energy distribution both inside the bulk and along the surface and inside/outside of the laser absorption region. During the laser pulse [Fig. 4(a)], superthermal electrons are produced with a similar spectra at the surface tip and inside the bulk with a slightly higher bulk temperature, but do not extend into the wings. In comparison, 1.3 ps later [Fig. 4(b)], after the ~MeV electrons have escaped, there remains a hotter, thermal distribution of lower energy electrons (~100 keV), which reflects the lower energy part of the original hot-electron spectrum being confined to the tip by the resistive wall fields and a shift to higher energies in the initially cold bulk electron population by heating. The cold wings show the slow diffusion of fast electrons from the tip.

In summary, we have shown that microcones irradiated with high-contrast light exhibit a confinement of hot electrons within a reduced volume at the cone tip, resulting in enhanced K_α fluorescence and bulk material temperatures. These funnel-shaped cones reveal similar hot-electron localization and material heating as small RMTs, reaching peak thermal temperatures of order ~200 eV. The observed electron confinement and heating is consistent with collisional PIC simulations and is attributed to the presence of strong resistive magnetic fields forming within the cone curvature. Although further work is required to characterize the temporal and spatial evolution of microcone heating, the enhanced coupling efficiency, the magnetic field structure, and the ability to create complex target shapes provide an advantage for future applications. The magnetic field structure largely separates the laser absorption region from the heated tip, which may enable isochoric heating of samples within a microenclosed tip. Moreover, the escape of the ~MeV electrons from the heated tip may slow the rate of energy loss to accelerated ions and surface plasma expansion, allowing for the production of intense ps-pulses of secondary particles and radiation like a broadband thermal backlighter or DD fusion neutron source.

This work was supported by the EU TMR laser Facility Access Program within the LASERLAB activities (Grants No. LULIACCESSHPRI-1999-CT 00052 and No. RII3-CT-2003-506350), by Grant No. E1127 from Région Ile-de-France, by University of Nevada, Reno under DOE/NNSA and OFES Grants No. DE-FC52-01NV14050, No. DE-FG02-05ER54837, and No. DE-FC02-04ER54789. The authors thank C. Back (General Atomics) for RMTs.

[1] B. A. Remington *et al.*, Science **284**, 1488 (1999).
[2] M. Tabak *et al.*, Phys. Plasmas **1**, 1626 (1994).
[3] R. Kodama *et al.*, Nature (London) **412**, 798 (2001).
[4] M. Nantel *et al.*, Phys. Rev. Lett. **80**, 4442 (1998).
[5] K. Eidmann *et al.*, J. Quant. Spectrosc. Radiat. Transf. **81**, 133 (2003).
[6] R. Stephens *et al.*, Phys. Rev. E **69**, 066414 (2004).
[7] A. Saemann, K. Eidmann, I. E. Golovkin, R. C. Mancini, E. Andersson, E. Forster, and K. Witte, Phys. Rev. Lett. **82**, 4843 (1999).

[8] G. Gregori *et al.*, Contrib. Plasma Phys. **45**, 284 (2005).
[9] W. Theobald *et al.*, Phys. Plasmas **13**, 043102 (2006).
[10] J. Myatt *et al.*, Phys. Plasmas **14**, 056301 (2007).
[11] Y. Sentoku *et al.*, J. Phys. IV **133**, 521 (2006).
[12] Y. Sentoku *et al.*, Phys. Plasmas **11**, 3083 (2004).
[13] R. Kodama *et al.*, Nature (London) **432**, 1005 (2004).
[14] Z. L. Chen, R. Kodama, M. Nakatsutsumi, H. Nakamura, M. Tampo, K. A. Tanaka, Y. Toyama, and T. Tsutsumi, Phys. Rev. E **71**, 036403 (2005).
[15] J. Rassuchine *et al.*, Med. Phys. **33**, 2251 (2006).
[16] M. Nakatsutsumi *et al.*, Phys. Plasmas **14**, 050701 (2007).
[17] L. Van Woerkom *et al.*, Phys. Plasmas **15**, 056304 (2008).
[18] J. S. Green *et al.*, Nat. Phys. **3**, 853 (2007).
[19] S. Baton *et al.*, Phys. Plasmas **15**, 042706 (2008).
[20] T. Pikuz *et al.*, Laser Part. Beams **19**, 285 (2001).
[21] J. Koch *et al.*, Rev. Sci. Instrum. **74**, 2130 (2003).
[22] E. Martinolli *et al.*, Rev. Sci. Instrum. **75**, 2024 (2004).
[23] E. Martinolli *et al.*, Phys. Rev. E **73**, 046402 (2006).
[24] A. Zhidkov, A. Sasaki, T. Utsumi, I. Fukumoto, T. Tajima, F. Saito, Y. Hironaka, K. G. Nakamura, K. I. Kondo, and M. Yoshida, Phys. Rev. E **62**, 7232 (2000).
[25] H. K. Chung *et al.*, High Energy Density Phys. **1**, 3 (2005).
[26] F. N. Beg *et al.*, Phys. Plasmas **4**, 447 (1997).
[27] Y. Sentoku and A. Kemp, J. Comput. Phys. **227**, 6846 (2008).
[28] L. Gremillet, G. Bonnaud, and F. Armiranoff, Phys. Plasmas **9**, 941 (2002).
[29] T. Taguchi, T. M. Antonsen, and K. Mima, Comput. Phys. Commun. **164**, 269 (2004).
[30] Y. Sentoku *et al.*, Phys. Plasmas **14**, 122701 (2007).